ACS OMEGA

http://pubs.acs.org/journal/acsodf

Article

One-Step Fabrication of the ZnO/g-C_3N_4 Composite for Visible Light-Responsive Photocatalytic Degradation of Bisphenol E in Aqueous Solution

Mahmudul Hassan Suhag,* Aklima Khatun, Ikki Tateishi, Mai Furukawa, Hideyuki Katsumata, and Satoshi Kaneco*

Cite This: *ACS Omega* 2023, 8, 11824−11836

Read Online

ACCESS | Metrics & More | Article Recommendations | Supporting Information

ABSTRACT: The ZnO/g-C_3N_4 composite was successfully synthesized by a simple one-step calcination of a urea and zinc acetate mixture. The photocatalytic activity of the synthesized composite was evaluated in the degradation of bisphenol E (BPE). The morphology, crystallinity, optical properties, and composition of the synthesized composite were characterized by using various analytical techniques such as scanning electron microscopy (SEM), transmitted electron microscopy (TEM), field emission-electron probe microanalysis (FE-EPMA), nitrogen adsorption and desorption isotherm measurement, Fourier-transform infrared (FTIR) spectroscopy, X-ray powder diffraction (XRD), diffuse reflectance spectroscopy (DRS), photoluminescence (PL) spectroscopy, electrochemical impedance spectroscopy (EIS), X-ray photoelectron spectroscopy (XPS), and thermogravimetric analysis (TGA). The degradation rate of BPE with the ZnO/g-C_3N_4 composite was 8 times larger than that obtained with pure g-C_3N_4 at the optimal conditions. The excellent photocatalytic activity was attributed to the synergistic effect between the g-C_3N_4 and ZnO, which enhanced the efficiency of charge separations, reduced the e^-/h^+ pairs recombination, and increased the visible light absorption ability. The radical scavenger studies indicated that the $^{\bullet}O_2^-$ and h^+ species were mainly responsible for the degradation of BPE. The stability test suggested the chemical and photostability of the synthesized composite. Two possible photocatalytical mechanisms have been suggested.

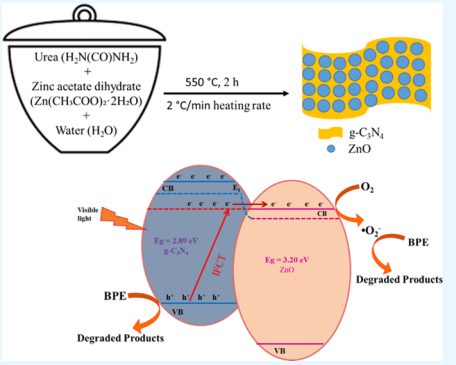

INTRODUCTION

Bisphenols are endocrine-disrupting chemicals that are widely used in the production of high-temperature composite materials in various polycarbonate plastics, rubber, epoxy resins, aerospace, and electronics industries.[1,2] Solutions of bisphenol compounds even at small concentrations cause hormonal anomalies and disrupt the reproductive growth activities and cancer.[3,4] The most widely used bisphenol compound, bisphenol A (BPA), is considered a threat to humans and animals due to its toxicity.[5] Therefore, BPA has been banned in several countries since a few years.[1] Another bisphenol compound, BPE, has become an alternative for BPA due to its similar properties and is being extensively used industrially.[1] However, BPE is also reported as a toxic compound and has significant estrogenic activity.[6] Thus, it is a matter of public health issue that needs an urgent response. It is necessary to develop a treatment technique for the unused or remaining BPE during the production process before its discharge into the natural environment, especially surface water. Several types of chemical, biological, electrochemical, and photochemical methods are applied for the treatment of wastewater containing solutions of bisphenol compounds.[7−10]

Photocatalysis has been considered to be one of the effective methods for degradation of bisphenols[11] because the photocatalytic method with irradiation of visible light to degrade water pollutants is cost effective, clean, and sustainable compared to other wastewater treatment techniques.[12] A semiconductor material can produce electron−hole pairs by absorbing the photons of energy from sunlight. The generated electron−hole pairs can react with the target pollutant by redox reactions and degrade it. The energy of the absorbed photon depends on the band gap of the semiconductor.[12] Generally, photocatalytic reactions can depend on the surface area, pore size, electron−hole pair recombination, band gap position, and morphology of the photocatalysts.[13]

Recently, g-C_3N_4 has received great attention as an interesting photocatalyst for wastewater detoxification, hydrogen production, and photoreduction of CO_2 under visible light irradiation. Pure g-C_3N_4 possesses a moderate band gap of ∼2.7 eV, which enables it to be excited by visible light up to

Received: October 17, 2022
Accepted: January 5, 2023
Published: March 21, 2023

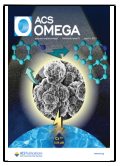

460 nm.[14−16] Furthermore, metal-free g-C_3N_4 has several features required for photocatalysis reactions, such as a π-conjugated electronic structure, layered crystal structure, low cost, nontoxic nature, high chemical and thermal stability, high electron conductivity, and facile fabrication.[15,17−22] However, the photocatalytic efficiency of g-C_3N_4 is greatly reduced because of the low quantum efficiency and fast recombination rate of the photogenerated electron−hole pairs.[14,23] Hence, to reduce the drawbacks of g-C_3N_4, several methods such as coupling with metal organic frameworks, covalent organic frameworks and other semiconductors (metal oxides and metal sulfides), doping with elements, and monitoring its structure and morphology have been proposed.[19,24−27] For instance, Kuila et al. reported the synthesis of cerium ion-adsorbed g-C_3N_4 for enhancing the photocatalytic degradation of methylene blue dye under sunlight irradiation.[28] de Sousa et al. prepared a ternary photocatalyst of ZnO/g-C_3N_4/carbon xerogel, which was used in efficient photocatalytic degradation of 4-chlorophenol under visible light irradiation.[29] Zhang et al. prepared a novel porous g-C_3N_4($[Mo_7O_{24}]^{6-}$·pCN) catalyst for improving the photocatalytic degradation of BPA and 4-chlorophenol.[30]

On the other hand, ZnO is a promising photocatalyst for degradation of organic and inorganic pollutants in wastewater due to its low price, nontoxicity, chemical stability, and high photocatalytic activity.[16,21,31] However, ZnO possesses a higher band gap of ∼3.2 eV and is active only in the ultraviolet region. ZnO has almost no activity in the visible region.[31,32]

It is a good strategy to prepare a composite with two photocatalysts by suitable matching of band-level positions for decreasing the electron−hole pair recombination. For example, Kumbhakar et al. reported the synthesis of a ZnO-anchored reduced graphene oxide nanocomposite via a simple hydrothermal treatment for superior photocatalytic degradation of dyes and tea stain on cotton fabrics.[33] Due to appropriate band alignment, the composite of ZnO containing a wider band gap with g-C_3N_4 containing a medium band gap (ZnO/g-C_3N_4) might generate an admirable heterostructure to progress charge separation.[34,35]

Many research works have been reported on the synthesis of the ZnO/g-C_3N_4 composite by several methods such as the chemisorption method, ball milling method, calcination method, reflux method, electrospinning method, reflux and vapor condensation method, deposition-precipitation method, monolayer dispersion method, and ultrasonic dispersion method. Excellent photocatalytic activity of the synthesized composites on the degradation of organic pollutants in wastewater has also been reported.[31,36−43] For instance, Gayathri et al. prepared a g-C_3N_4-based ZnO nanocomposite via a precipitation-assisted thermal condensation method, which was used in enhanced photocatalytic degradation of methylene blue and acid blue 113 dyes under sunlight irradiation.[44] Zhang et al. reported the synthesis of a ZnO/g-C_3N_4 composite microsphere via a self-assembly method followed by calcination in the air for effective photocatalytic degradation of methyl orange and tetracycline under visible light irradiation.[22] However, few works have reported on the fabrication of the ZnO/g-C_3N_4 composite by simple and convenient methods. Furthermore, the degradation of the endocrine-disrupting material BPE with the ZnO/g-C_3N_4 composite under visible light irradiation has been not reported yet.

In the present work, the ZnO/g-C_3N_4 composite has been synthesized by a very facile calcination technique using zinc acetate and urea as precursors of ZnO and g-C_3N_4, respectively. The photocatalytic degradation of BPE with the simply synthesized ZnO/g-C_3N_4 composite under visible light radiation has been investigated. The different parameters such as ZnO amount in the composite, synthesis and calcination conditions, amount of ZnO/g-C_3N_4 composite, initial concentration of BPE, and solution pH have been optimized for the photocatalytic degradation. Furthermore, the ZnO/g-C_3N_4 composite was characterized by using several techniques. In addition, photocatalytic experiments using different radical scavengers were done to assess the probable reaction pathway.

MATERIALS AND METHODS

Materials. 1,1-Bis(4-hydroxyphenyl)ethane (BPE, 98.0%), urea (99.0%) and zinc acetate dihydrate (99.0%), isopropyl alcohol (IPA, 99.7%), ethylenediaminetetraacetic acid (EDTA, 98.0%) benzoquinone (BQ, 98.0%), sodium hydroxide (97.0%), and nitric acid (61%) were purchased from FUZIFILM Wako Pure Chemical Corporation, Japan. Acetonitrile (99.5%) was obtained from Kanto Chemical Co., Inc., Japan. All of the chemicals were used without further purification. Pure water was obtained from an ultrapure water system (Advantec MFS Inc., Tokyo, Japan).

Synthesis of the ZnO/g-C_3N_4 Composite. The composite of ZnO/g-C_3N_4 was synthesized by a facile one-step calcination of the mixture of urea and zinc acetate dihydrate (Figure S1). Typically, 20 g of urea and 2 g of zinc acetate were mixed and dispersed with 5 mL of water in a 30 mL crucible with a lid. Then, the crucible was covered by an aluminum foil, placed in a muffle furnace, heated to 550 °C at a heating increment rate of 2 °C min^{-1}, and held for 2 h at 550 °C as the calcination temperature. Finally, the sample was manually ground in an agate mortar into a light-yellow powder. Pure ZnO and g-C_3N_4 were synthesized from zinc acetate and urea by the same method, respectively. The stepwise urea and zinc acetate decomposition during the formation of g-C_3N_4 and ZnO, respectively, is illustrated in Figure S1.[45−47]

Characterization. The ZnO/g-C_3N_4 composite, g-C_3N_4, and ZnO were characterized by thermogravimetric analysis (TGA), Fourier-transform infrared (FTIR), X-ray powder diffraction (XRD), X-ray photoelectron spectroscopy (XPS), scanning electron microscopy (SEM), transmitted electron microscopy (TEM), field emission-electron probe micro-analysis (FE-EPMA), UV−vis diffuse reflectance spectroscopy (DRS), photoluminescence (PL), electrochemical impedance spectroscopy (EIS), and nitrogen adsorption and desorption isotherm analysis. TGA of the prepared composite was performed in air at a heating rate of 10 °C min^{-1} on the SII (EXSTAR 6000, TG/DTA 6200) thermal analysis system with the temperature ranging from 25 to 950 °C. The FTIR spectra of the photocatalysts were recorded using a SPECTRUM 100 FTIR spectrometer (Perkin Elmer) with an attenuated total reflection (ATR) assembly. XRD measurements were performed using a Rigaku RINT Ultima-IV diffractometer by Cu Kα radiation at a scan rate of 0.04° s^{-1} in the scan range of 10−80°. XPS characterization of the photocatalysts was performed using a PHI Quantera SXM photoelectron spectrometer with Al Kα radiation. SEM and TEM images of photocatalysts were used to analyze the surface morphology by using a Hitachi S-4000 SEM and a JEOL JEM-1011 TEM, respectively. FE-EPMA images of the composite were used to

https://doi.org/10.1021/acsomega.2c06678
ACS Omega 2023, 8, 11824−11836

analyze the elemental mapping by using a JEOL JX-A-8530F FE-EPMA. The specific surface area, average pore size, and total pore volume of the photocatalysts were estimated from the N_2 adsorption−desorption isotherm using the BELSORP-miniII (MicrotracBEL) apparatus with the Brunauer−Emmett−Teller (BET) equilibrium equation and Barrett−Joyner−Halenda (BJH) analysis. The UV−vis DRS of the photocatalysts was done by a JASCO V-750 UV−vis instrument equipped with an integrating sphere attachment. Photoluminescence (PL) spectra of the photocatalysts were obtained with a Shimadzu RF-5300PC system with an excitation wavelength of 360 nm. The EIS measurement of the photocatalysts was performed using an electrochemical Versa STAT 3 workstation (Princeton Applied Research) equipped with a conventional three-electrode system. A uniform photocatalyst slurry with nafion solution was coated on a fluorine-doped tin oxide (FTO) glass plate to prepare the working electrode, and a 0.5 mol L^{-1} Na_2SO_4 aqueous solution was used as the electrolyte.

Photocatalytic Degradation. The photocatalytic degradation of BPE by the synthesized ZnO/g-C_3N_4 composite was carried out up to 3 h with visible light irradiation at ambient temperature. A Pyrex glass cell (inner volume, 50 mL) was used for photocatalytic degradation. Typically, 30 mL of a 3 ppm BPE solution and 30 mg of the ZnO/g-C_3N_4 composite were added to the glass cell and magnetically stirred before and during irradiation. Before irradiation, the photocatalyst suspension containing BPE was allowed to reach adsorption−desorption equilibrium for 30 min in the dark. Then, the BPE solution was irradiated with a light-emitting diode (LED) lamp (TOSHIBA LDA14L-G/100W) with a UV (400 nm) cutoff filter (Y-44, HOYA), which was placed on one side of the reaction cell. During the degradation, 1.5 mL of the suspension was taken out at 30 min regular intervals and centrifuged at 10,000 rpm for 5 min to separate the photocatalyst. Then, the supernatant was analyzed for BPE concentration determination. The amount of BPE in the solution was measured using a high-performance liquid chromatograph equipped with a SHIMADZU UV/Vis detector (UV 7750) and a separation column ODS-2 (GL Science Inc.). The chromatogram was monitored at a wavelength of 274 nm. The mobile phase consisted of a solvent mixture of acetonitrile and water (60:40, v/v) in isocratic mode. The flow rate of the mobile phase was 1.0 mL min^{-1}. The photocatalytic degradation of BPE by the synthesized bare g-C_3N_4 and bare ZnO was also carried out at similar degradation conditions. Moreover, the degradation in the absence of photocatalysts (photolysis) was also carried out under similar degradation conditions. To determine the optimum condition for degradation of BPE by the synthesized ZnO/g-C_3N_4 composite, the effect of operating conditions such as ZnO amount in the composite, calcination condition of the composite synthesis, photocatalyst amount, initial BPE concentration, and initial pH of the solution were also investigated. To inspect the role of reactive species in photocatalytic degradation of BPE with the ZnO/g-C_3N_4 composite, three scavenger tests were carried out in the same optimal condition. In the scavenger tests, solutions of IPA, EDTA, and BQ were used as $^{\bullet}OH$, h^+ and $^{\bullet}O_2^-$ radical scavengers, respectively. The reusability of the ZnO/g-C_3N_4 composite for photodegradation of BPE was studied.

In addition, the kinetics and reaction rate of the photocatalytic degradation process were studied according to the Langmuir−Hinshelwood (L−H) model, which was developed by Turchi and Ollis.[48] The model was expressed as eq 1,

$$r_0 = -\frac{dC}{dt} = \frac{kKC}{1 + KC} \quad (1)$$

where r_0 is the degradation rate in the reaction, k is the rate constant, and K and C are the adsorption equilibrium constant and reactant concentration, respectively. If the initial concentration C_0 is very small, it can be simplified to eq 2.

$$-\ln\left(\frac{C}{C_0}\right) = kKt = k_{obs}t \quad (2)$$

The equation becomes a linear expression on time t with respect to $\ln(C/C_0)$, where k_{obs} is the reaction rate constant. The values of k_{obs} were calculated by plotting $\ln(C/C_0)$ versus t.

RESULTS AND DISCUSSION

TG Analysis. In order to understand the thermal stability and amount of ZnO content in the prepared ZnO/g-C_3N_4 composite, TG analysis was carried out from 25 to 950 °C at a heating increment rate 10 °C min^{-1}. It was reported that ZnO is very stable till more than 900 °C temperature.[19] There are two steps of weight loss in the TGA curve, as shown in Figure 1. The major weight loss was observed from 400 to 640 °C,

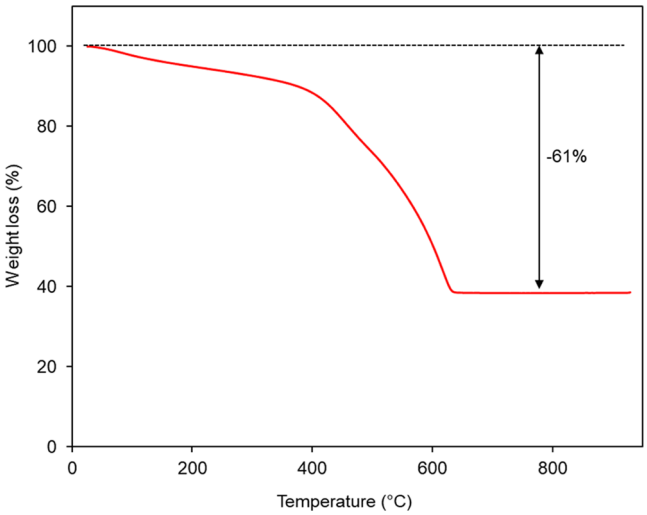

Figure 1. TG analysis curve of the ZnO/g-C_3N_4 composite.

which could be assigned to the combustion of the g-C_3N_4 composite.[19] The weight percentage of ZnO in the prepared composite was 38.9%, as observed in the case of 2 g for $(CH_3COO)_2Zn$.

FTIR Analysis. The formation of the ZnO/g-C_3N_4 composite was studied by FTIR spectroscopy. Figure 2 shows the corresponding FTIR spectra of the prepared ZnO, g-C_3N_4, ZnO/g-C_3N_4 composite, and ZnO/g-C_3N_4 composite after degradation of BPE. Pure C_3N_4 showed several peaks between 1200 and 1650 cm^{-1} associated with the different C−N stretching modes for the presence of the extended C_3N_4 arrangement.[15,49] The intense peak at 810 cm^{-1} was assigned to the out-of-plane vibration of the heterocyclic C−N bending mode of the triazine ring.[12] The broad band between 3000 and 3300 cm^{-1} appeared due to the stretching modes of the deformed N−H bond and −OH groups of the absorbed water

https://doi.org/10.1021/acsomega.2c06678
ACS Omega 2023, 8, 11824−11836

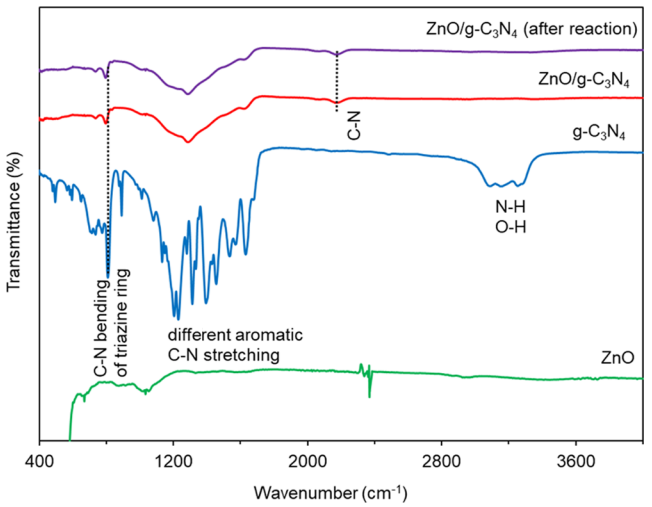

Figure 2. FTIR spectra of ZnO, g-C_3N_4, the ZnO/g-C_3N_4 composite, and the ZnO/g-C_3N_4 composite after the degradation reaction.

molecules.[50] The FTIR spectra of the prepared ZnO were not observed clearly, as shown in the figure. In the FTIR spectra of the ZnO/g-C_3N_4 composite, all characteristic peaks of g-C_3N_4 were observed. The intensities of the peaks observed at 1200−1650 cm^{-1} for different aromatic C−N stretching decreased and merged to a broad peak, compared to g-C_3N_4.[12] These results could be attributed to the existence of ZnO in the composite. Also, the peak for the out-of-plane vibration of the heterocyclic C−N bending mode of the triazine ring was red-shifted to a lower wavenumber at 794 cm^{-1} with smaller intensity, compared to the peak of g-C_3N_4. The result indicated the weakening of the bond strength of C═N and C−N due to lower conjugation of pure g-C_3N_4 and ZnO in the composite.[12] A weak peak was formed at 2204 cm^{-1} for the formation of the new C−N bond. ZnO may cleavage the triazine units and generate new C−N bonds from the sp^2 C−N bonds of the triazine units.[12] However, there were few peaks observed at 3000−3300 cm^{-1} compared to the spectra of pure g-C_3N_4. Despite the absence of the Zn−O stretching peak in the FTIR spectra, the above results supported the formation of a hybrid structure rather than a physical mixture of ZnO and g-C_3N_4. The peaks in the FTIR spectra of the ZnO/g-C_3N_4 composite did not change after the photocatalytic degradation of BPE, which indicated the chemical stability of the composite.

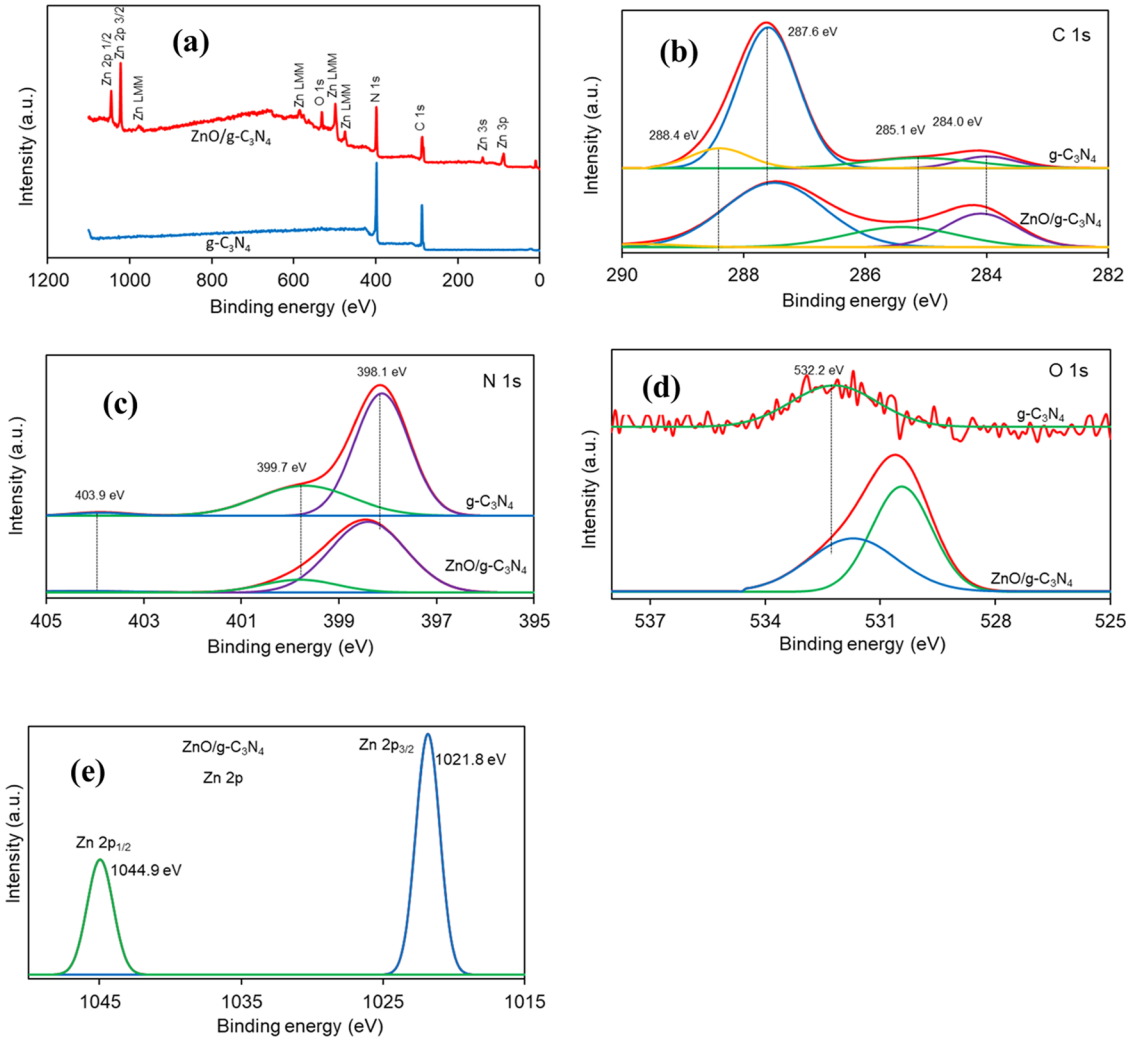

Figure 3. (a) Survey XPS spectra of g-C_3N_4 and the ZnO/g-C_3N_4 composite; overlapping high-resolution XPS (b) C 1s, (c) N 1s, and (d) O 1s spectra of g-C_3N_4 and the ZnO/g-C_3N_4 composite and (e) high-resolution XPS Zn 2p spectra of the ZnO/g-C_3N_4 composite.

https://doi.org/10.1021/acsomega.2c06678
ACS Omega 2023, 8, 11824−11836

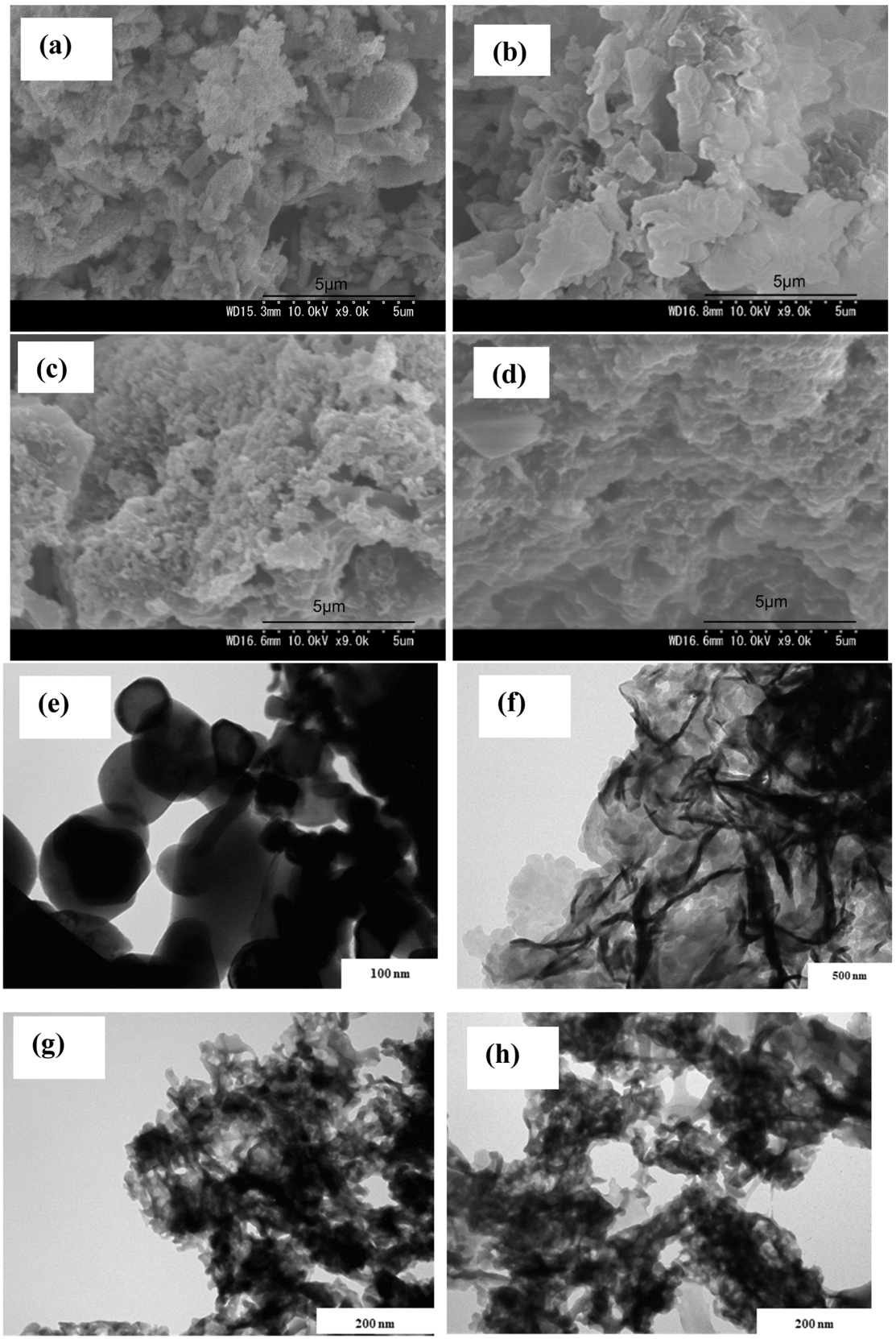

Figure 4. SEM images of (a) ZnO, (b) g-C_3N_4, (c) the ZnO/g-C_3N_4 composite, and (d) the ZnO/g-C_3N_4 composite after the degradation reaction; and TEM images of (e) ZnO, (f) g-C_3N_4, (g) the ZnO/g-C_3N_4 composite, and (h) the ZnO/g-C_3N_4 composite after the degradation reaction.

XRD Analysis. The XRD patterns of the prepared ZnO, g-C_3N_4, the ZnO/g-C_3N_4 composite, and the ZnO/g-C_3N_4 composite after the degradation reaction of BPE are shown in Figure S2. The 2θ values for the diffraction peak of the

https://doi.org/10.1021/acsomega.2c06678
ACS Omega 2023, 8, 11824−11836

Table 1. Surface Area, Pore Size and Pore Volume of the g-C_3N_4 and ZnO/g-C_3N_4 Composite

	BET			BJH		
photocatalyst	S (m^2 g^{-1})	V_{pore} (cm^3 g^{-1})	D_{pore} (nm)	S (m^2 g^{-1})	V_{pore} (cm^3 g^{-1})	D_{pore} (nm)
g-C_3N_4	52.9	0.270	16.7	60.9	0.225	2.59
ZnO/g-C_3N_4	10.4	0.051	19.5	8.26	0.0493	3.32

prepared ZnO sample were 31.76, 34.38, 36.22, 47.54, 56.60, 62.86, 66.52, 67.94, and 69.10° corresponding to the (100), (002), (101), (102), (110), (103), (200), (112), and (201) crystal planes are ascribed to the hexagonal wurtzite structure of ZnO, respectively.[24] Furthermore, the 2θ values for the diffraction peak of the prepared g-C_3N_4 sample were 13.01 and 27.8° corresponding to the (100) and (002) planes, respectively. The intense peak of 27.8° is related to the interlayer C−N stacking of the conjugated aromatic system and the weak peak of 13.01° corresponds to the periodic arrangement of the s-triazine units. The observed results are consistent with the reported literature.[20,51]

A broad peak with low intensity at a 2θ value of around 27° was observed for the XRD pattern of the ZnO/g-C_3N_4 composite, which indicates that the ZnO could restrict the g-C_3N_4 crystal growth and that the innate structure of the pure g-C_3N_4 could not be retained well.[12] However, any peak for ZnO was not present in the pattern. This result showed the lower crystallization of the composite. It can be suggested that ZnO and g-C_3N_4 lost their crystallinity upon the composite formation and that the ZnO/g-C_3N_4 composite existed in an amorphous state. The same XRD pattern was also observed for the ZnO/g-C_3N_4 composite after the degradation reaction. The crystalline size of the photocatalysts from the diffraction peaks of the full width at half-maximum (FWHM) was determined by using Scherrer's equation. It was speculated that the crystalline sizes of ZnO and g-C_3N_4 are 42 and 8.7 nm, respectively.

XPS Analysis. XPS measurement was taken to investigate the surface chemical composition and interaction between the ZnO and g-C_3N_4 in the prepared composite. The survey XPS spectra of the prepared g-C_3N_4 and ZnO/g-C_3N_4 composite are shown in Figure 3a. C and N elements were detected in both the survey spectra. In addition, Zn and O were detected in the spectra of the ZnO/g-C_3N_4 composite.[44,52] The results confirmed the association of ZnO with g-C_3N_4 and the purity of the composite. The overlapping high-resolution C 1s, N 1s, and O 1s XPS spectra of g-C_3N_4 and the ZnO/g-C_3N_4 composite are shown in Figure 3b−d and the high-resolution Zn 2p XPS spectra of the ZnO/g-C_3N_4 composite are shown in Figure 3e. The high-resolution C 1s XPS spectrum of g-C_3N_4 can be deconvoluted into four components located at 287.6, 285.1, 284, and 288.4 eV, which are related to the N=C−N groups of the s-triazine ring, sp^3 C−N bond, sp^2 C=C bond, and C−O groups induced by unavoidable oxidation of the sample, respectively[53] (Figure 3b). As shown in Figure 3c, the high-resolution XPS N 1s spectrum of g-C_3N_4 was fitted by the three peaks of 403.9, 399.7, and 398.1 eV, which can be ascribed to the sp^2N (C=N−C) involved in the triazine ring, tertiary nitrogen atom (NC_3), or secondary nitrogen atom (HNC_2), and the charging effects or positive charge localized in the heterocycles, respectively.[54] Moreover, the position and relative intensity of the peaks in the high-resolution C 1s and N 1s XPS spectra of the ZnO/g-C_3N_4 composite were changed,[51,53] as shown in Figure 3b,c. Furthermore, the high-resolution O 1s XPS spectra of g-C_3N_4 showed one peak at 532.2 eV, which is assigned to the surface −OH groups on the g-C_3N_4 or in the adsorbed H_2O.[54] In contrast, the high-resolution O 1s XPS spectra of ZnO/g-C_3N_4 illustrated two peaks at 530.9 and 531.9 eV for O_2^{2-} in the ZnO wurtzite structure and surface −OH groups adsorbed on the composite, respectively (Figure 3d).[50] In the case of the high-resolution Zn 2p XPS spectrum of the ZnO/g-C_3N_4 composite, as shown in Figure 3e, the binding energy values of Zn $2p_{3/2}$ and Zn $2p_{1/2}$ were located at 1021.8 and 1044.9 eV, representing the Zn^{2+} oxidation state of the ZnO material, respectively. Furthermore, the difference between the two binding energy peaks was about 23.1 eV. The results proved to be in good match with the reported ZnO binding energy values in the ZnO/g-C_3N_4 composite.[55] In addition, the structure of the Zn LMM Auger peaks in the survey spectrum of ZnO/g-C_3N_4 composite revealed the presence of Zn−N bonds[51] (Figure 3a). Thus, the XPS analysis further confirmed the existence of ZnO in the composite.

Morphological Study. The formation of the ZnO/g-C_3N_4 composite was investigated by SEM and TEM analysis of ZnO, g-C_3N_4, and the ZnO/g-C_3N_4 composite. Figure 4 shows the SEM and TEM images of ZnO, g-C_3N_4, and the ZnO/g-C_3N_4 composite after degradation of BPE. The SEM image of the prepared ZnO (Figure 4a) showed the irregular surface morphology with different sizes and shapes of particles. The ZnO particles had a combination of rod-like, semispherical, and flower-like structures with different sizes. Figure 4b illustrates the sheet-like structure of g-C_3N_4. From Figure 4c, it can be seen that the composite was composed of flower-like ZnO and sheet-like g-C_3N_4. The TEM image showed the random arrangement of ZnO particles with semispherical or hexagonal shape (Figure 4e). The pure g-C_3N_4 had a sheet-like structure in the TEM analysis (Figure 4f). For the composite, it was observed that ZnO particles were imbedded in the g-C_3N_4 sheet, as shown in Figure 4g. Hence, ZnO could be inserted into the g-C_3N_4 sheet successfully. The composite may be expected to reduce the electron−hole pair recombination rate and to increase the photocatalytic degradation efficiency under visible light.[24] Elemental mapping of N, C, Zn, and O of the ZnO/g-C_3N_4 composite was observed by FE-EPMA. Figure S3 proves the uniform distribution of all elements through the whole composite. From the SEM and TEM images, it was also observed that the surface morphology of the composite could not change significantly after the degradation of BPE (Figure 4d,h). The stability and proficiency of the ZnO/g-C_3N_4 composite is indicated.

BET and BJH Analysis. In order to investigate the porous structure and surface area of g-C_3N_4 and the ZnO/g-C_3N_4 composite, the nitrogen adsorption−desorption isotherm was measured. Figure S4a,b shows the nitrogen adsorption−desorption isotherm curve and pore size distribution curve of the materials, respectively. As shown in Figure S4a, the adsorption isotherms of g-C_3N_4 and the ZnO/g-C_3N_4 composite corresponded to type IV with H3 hysteresis loops. The results indicated the mesoporous structure of g-C_3N_4 and the ZnO/g-C_3N_4 composite.[56] The surface area, average pore

https://doi.org/10.1021/acsomega.2c06678
ACS Omega 2023, 8, 11824−11836

diameter, and total pore volume of g-C_3N_4 and the ZnO/g-C_3N_4 composite are presented in Table 1 by BET and BJH analysis. It was observed that the surface area and pore volume were decreased and the pore diameter was increased, owing to the formation of the ZnO/g-C_3N_4 composite from g-C_3N_4. The growth of ZnO might be loaded into the pores of g-C_3N_4, which could strengthen the interfacial structure of ZnO and g-C_3N_4.[57] A lower surface area and pore volume and higher pore diameter of the ZnO/g-C_3N_4 composite were also previously reported, compared to g-C_3N_4.[22]

DRS Analysis. The photocatalytical activity depends on the optical properties. Hence, to investigate the light absorption properties of the prepared ZnO, g-C_3N_4, and the ZnO/g-C_3N_4 composite, the UV−vis DRS was measured at room temperature. Figure 5a shows the Kubelka-Munk function of the UV−vis DRS of the prepared ZnO, g-C_3N_4, and the ZnO/g-C_3N_4 composite after the degradation reaction of BPE. It was observed that the prepared ZnO and g-C_3N_4 had the absorption edge at about 390[15] and 430 nm,[54] respectively. Moreover, the absorption edge of the prepared ZnO/g-C_3N_4 composite was significantly red-shifted to a higher wavelength compared to both pure ZnO and g-C_3N_4.[20] The results suggested the higher absorption and utilization of visible light capacity by the prepared ZnO/g-C_3N_4 composite. The optical band gap of the prepared ZnO, g-C_3N_4, and ZnO/g-C_3N_4 composite was calculated by Tauc equation.

$$ah\nu = A(h\nu - E_g)^n \quad (3)$$

where α, h, υ, A, and E_g are the absorption coefficient, Planck's constant, light frequency, characteristic constant, and band gap energy, respectively. The value of n depends on the transition in a semiconductor: $n = 1/2$ for direct transition and $n = 2$ for indirect transition. The indirect band gap of g-C_3N_4 and the ZnO/g-C_3N_4 composite was determined by plotting the value of $(\alpha h\nu)^{1/2}$ vs $h\nu$ (Figure S5a). On the other hand, ZnO has direct transition; hence, the band gap of ZnO was calculated by plotting the value of $(\alpha h\nu)^2$ vs $h\nu$ (Figure S5b).[22,24] The calculated band gaps for ZnO, g-C_3N_4, and the ZnO/g-C_3N_4 composite are 3.20, 2.89, and 2.22 eV, respectively. The lower band gap of the composite compared to the pure ZnO and g-C_3N_4 supported the higher charge separation and better photocatalytic activity of the composite. Furthermore, the absorption edge in the Kubelka-Munk function of UV−vis DRS and the band gap of the ZnO/g-C_3N_4 composite could not change meaningfully after the treatment of BPE, which indicated the chemical stability of the composite.

PL Analysis. The PL intensity is directly proportional to the electron−hole pairs recombination rate. Hence, PL spectra are one of the most effective parameters for investigation of the photogenerated electron−hole pairs migration, transfer, and recombination of photocatalysts.[18,22] Figure 5b shows the PL emission spectra of ZnO, g-C_3N_4, and the ZnO/g-C_3N_4 composite after the degradation reaction of BPE in the range from 410 to 750 nm upon excitation at 360 nm. It was seen that the PL intensity of the ZnO/g-C_3N_4 composite was significantly reduced relative to that of both ZnO and g-C_3N_4. The results indicated the higher efficient electron transfer from the valence band to the conduction band as well as the lower electron−hole pair recombination. The recombination rate of electron−hole pairs could be reduced by the synergic effect between the ZnO and g-C_3N_4 components.[34] In addition, the PL intensity of the ZnO/g-C_3N_4 composite remained almost

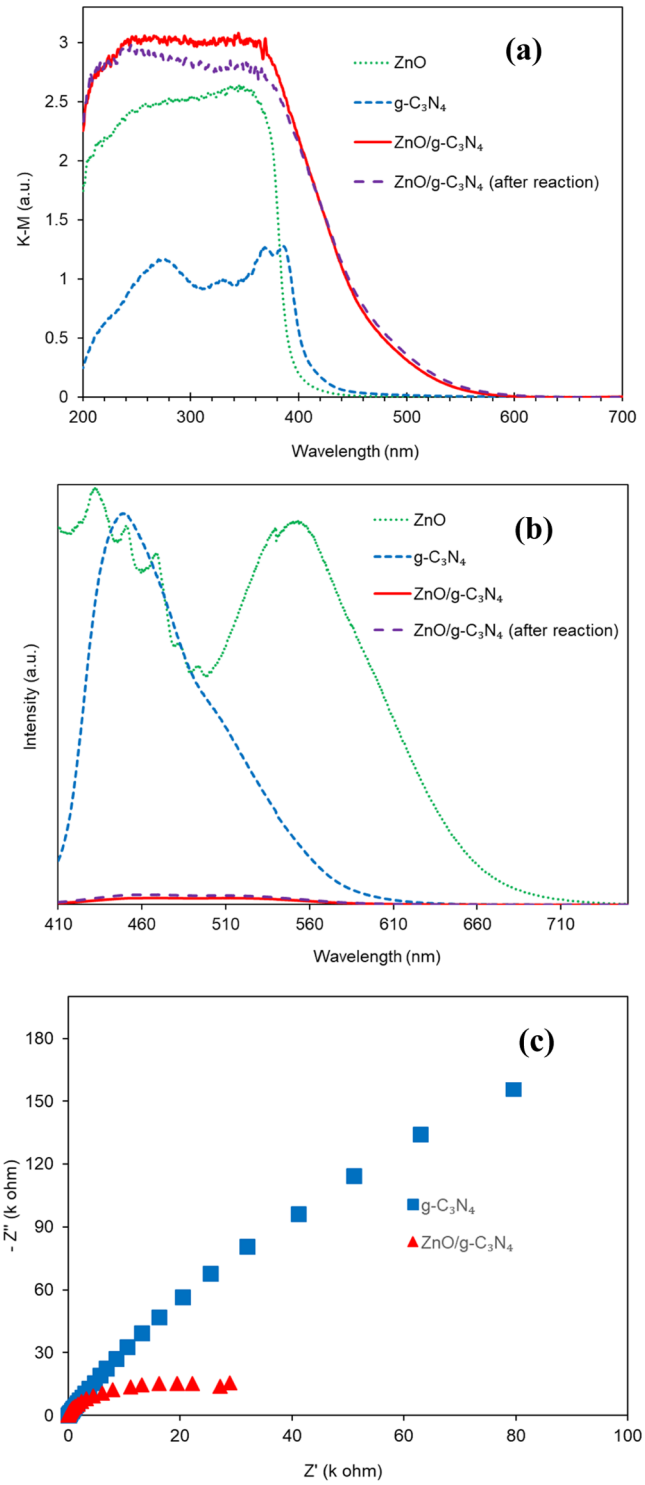

Figure 5. (a) Kubelka-Munk function of UV−vis DRS and (b) PL spectra (upon the excitation at 260 nm wavelength) of the prepared ZnO, g-C_3N_4, and the ZnO/g-C_3N_4 composite after the degradation reaction; and (c) EIS Nyquist plots of g-C_3N_4 and ZnO/g-C_3N_4.

the same after the degradation of BPE. The observation implicated the stability of the composite.

EIS Analysis. To analyze the photogenerated charge transfer and migration efficiency of the photocatalysts, the EIS analysis was conducted. Usually, a smaller semicircle radius in the EIS Nyquist plot suggests a lower charge transfer resistance across the photoelectrode surface.[22] Figure 5c shows

https://doi.org/10.1021/acsomega.2c06678
ACS Omega 2023, 8, 11824−11836

the EIS Nyquist plots for g-C_3N_4 and the ZnO/g-C_3N_4 composite. It was observed that the ZnO/g-C_3N_4 composite exhibited a smaller semicircle radius than the g-C_3N_4 electrode. The result indicated the higher photoinduced electron−hole transfer and migration, which supports a better photocatalytic activity of the ZnO/g-C_3N_4 composite.

Photocatalytic Activity. The photocatalytic activity of the ZnO/g-C_3N_4 composite on degradation of BPE with visible light irradiation is shown in Figure 6. For comparison, the

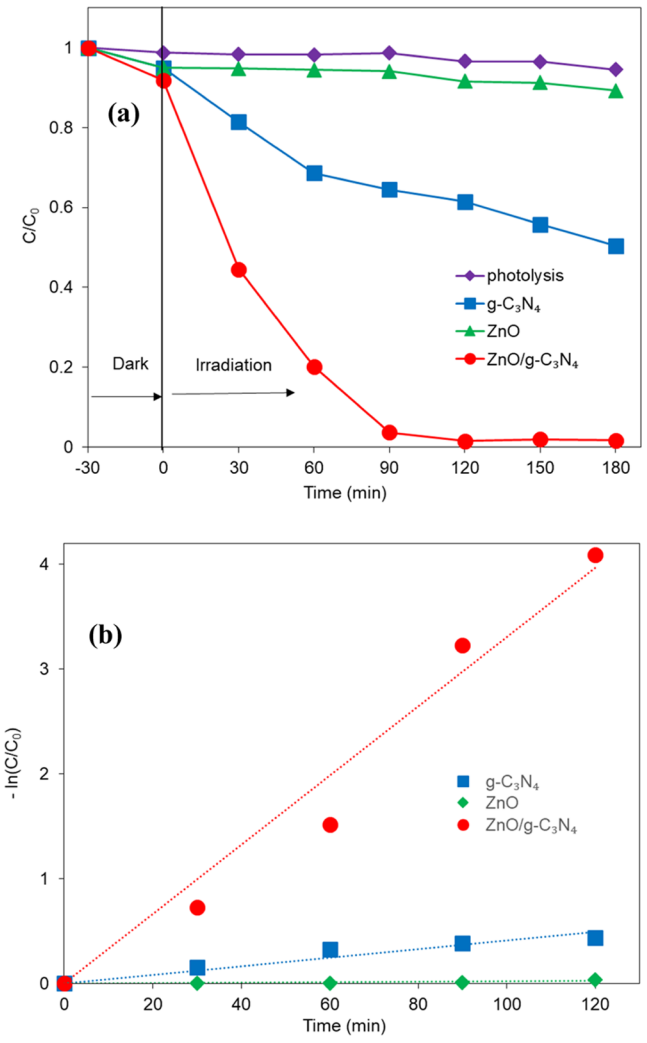

Figure 6. (a) Photocatalytic degradation of BPE with different catalysts under visible light irradiation and (b) the plot of $-\ln(C/C_0)$ versus irradiation time; BPE: 3 ppm (30 mL), photocatalyst: 30 mg.

photocatalytic activities of pure ZnO and g-C_3N_4 are also illustrated. Furthermore, the photolysis properties of BPE have been studied. The results indicated that BPE is very stable under visible light irradiation without any photocatalyst. The ZnO exhibited almost no degradation of BPE due to its limited visible light absorption. Furthermore, the ZnO/g-C_3N_4 composite showed a superior photocatalytic activity than g-C_3N_4. The rate constant was calculated according to pseudo-first-order kinetics, as shown in Figure 6b. From Table 2, it was observed that the degradation rate of BPE with the ZnO/g-C_3N_4 composite was 8 times better than that obtained with pure g-C_3N_4.

Table 2. Kinetic Parameters for Photocatalytic Degradation of BPE

photocatalyst	rate constant (min^{-1})	$t_{1/2}$ (min)	R^2
ZnO	0.2×10^{-3}	3465	0.67
g-C_3N_4	4.1×10^{-3}	169	0.92
ZnO/g-C_3N_4	3.3×10^{-2}	21	0.97

Effect of ZnO Amount. To study the effect of ZnO amount in the ZnO/g-C_3N_4 composite on the photocatalytic degradation of BPE, different composites of ZnO/g-C_3N_4 were prepared by varying the zinc acetate amount (0.1, 0.2, 0.5, 1.0, 2, and 2.5 g) with 20 g of urea. Figure S6 shows the photocatalytic degradation of BPE with the ZnO/g-C_3N_4 composites by varying the amount of ZnO (different amounts of zinc acetate in the preparation of the composite). It can be found that the composite prepared from 20 g of urea and 2 g of zinc acetate showed maximum photocatalytic activity. The photocatalytic degradation was enhanced on increasing the amount of zinc acetate from 0.1 to 2.0 g as the precursor of ZnO in the composite and was decreased on further increasing the amount of zinc acetate (Figure S6 and Table S1). It means that the optimal amount of zinc acetate was 2 g with 20 g of urea to prepare the ZnO/g-C_3N_4 composite for photocatalytic degradation of BPE. The enhancement of photogenerated electron−hole separation by the synergistic effect between ZnO and g-C_3N_4 could be responsible for the better photocatalytic degradation of BPE.[55] However, excess ZnO may produce electron−hole pairs recombination site and reduce the photoinduced charge separation.[50]

Effect of Calcination Process. In order to understand the effect of the calcination process to prepare ZnO/g-C_3N_4 composite on the photocatalytic degradation of BPE, the composite was prepared by a two-step calcination process with different intermediate calcination temperatures. Before the calcination of the mixture of zinc acetate and urea at 550 °C temperature for 2 h, it was additionally calcined at 100, 200, and 300 °C temperature for 2 h as the intermediate calcination step to prepare different composites. Figure S7 shows the photocatalytic degradation of BPE with ZnO/g-C_3N_4 composites prepared at one-step and different two-step calcination processes. It can be seen that the composite prepared in the direct one-step calcination at 550 °C temperature showed maximum photocatalytic activity (Figure S7 and Table S2). It means that the optimal conditions of composite preparation were direct one-step calcination at 550 °C temperature for 2 h.

Effect of Catalyst Dosage. It is known that the catalyst dosage shows the impact on the photocatalytic reaction. The effect of ZnO/g-C_3N_4 dosage on the photocatalytic degradation of BPE under visible light irradiation was studied by varying the amount of ZnO/g-C_3N_4 between 5−50 mg. The results are presented in Figure S8. The degradation of BPE was increased on increasing the amount of ZnO/g-C_3N_4 up to 30 mg, which could be caused by increasing the number of active sites on the catalyst surface.[35] On further increasing the catalyst above 30 mg, the degradation of BPE was not increased significantly, which may be due to the increasing light-screening effect by the excess amount of the catalyst (Figure S8 and Table S3). For excess overdosage of ZnO/g-C_3N_4, the number of active sites of ZnO/g-C_3N_4 may remain almost the same.[20] Therefore, 30 mg of ZnO/g-C_3N_4 was

https://doi.org/10.1021/acsomega.2c06678
ACS Omega 2023, 8, 11824−11836

selected as the optimal amount of photocatalyst for the present study.

Effect of Initial BPE Concentration. It is necessary to study the effect of the initial substrate concentration on the BPE photocatalytic degradation with ZnO/g-C_3N_4. The effect of the initial concentration of BPE was studied by varying it from 3 to 10 mg L^{-1}. The results are shown in Figure S9. It was found that as the initial BPE concentration increased from 3 to 10 mg L^{-1}, the degradation efficiency gradually decreased (Figure S9 and Table S4). Increase in the number of BPE molecules on the catalyst surface could be responsible for the decrement of photocatalytic degradation efficiency on increasing the concentration of BPE. This phenomenon explains why the degradation amount of BPE did not increase even when the substrate concentration increased from 3 to 10 mg L^{-1}. Simultaneously, the probabilities of the reactive species formation on the catalyst surface were also decreased.[24,35] Hence, 3 mg L^{-1} of BPE was selected to study the photodegradation of BPE with ZnO/g-C_3N_4 composite.

Effect of pH. The effect of pH is considered as an important factor during the photocatalytic degradation procedure. Therefore, the influence of initial pH on the degradation efficiency of BPE with ZnO/g-C_3N_4 was investigated in the pH range 2−10. As seen in Figure S10, the degradation efficiency increased on increasing the initial pH of the solution. However, the degradation at pH 8 was slightly worse relative to that at pH 6 (Figure S10 and Table S5). The dependence of the surface charge properties of the ZnO/g-C_3N_4 composite on the pH of the solution may affect the degradation of BPE.[3] In addition, at high initial pH, more hydroxide ions (OH^-) exist in the solution, which induce the generation of hydroxide free radicals ($^{\bullet}OH$). The photocatalytical degradation of BPE may be accelerated by the generated $^{\bullet}OH$ radicals.[10] Therefore, pH 6, which is actually the initial pH of the 3 mg L^{-1} BPE solution, was selected as the optimal pH to avoid unwanted chemical treatment for pH adjustment.

Scavenger Role. It is well known that holes (h^+), hydroxyl radicals ($^{\bullet}OH$), and superoxide anion radical anions ($^{\bullet}O_2^-$) are the reactive species that degrade the pollutants during the photocatalytic degradation reaction. Therefore, in order to understand the photocatalytic degradation mechanism of BPE with the ZnO/g-C_3N_4 composite, scavenging tests were performed by adding EDTA, BQ, and IPA corresponding to the h^+, $^{\bullet}O_2^-$, and $^{\bullet}OH$ radicals, respectively.[22] The results are shown in Figure 7 and Table 3. It was found that the presence of IPA slightly decreased the photocatalytic degradation of BPE compared to the case without the scavenger. On the other hand, BQ significantly influenced the photocatalytic degradation. In addition, EDTA impacted the degradation process moderately. The results suggested that $^{\bullet}O_2^-$ could be the major active species in the photocatalytic reaction and h^+ seems to play an important role in the photocatalytic activity of the ZnO/g-C_3N_4 composite, whereas the $^{\bullet}OH$ radical may play a minor part in the photocatalytic reaction of BPE. The results showed good agreement with the scavenger role of the photocatalytic degradation of methylene blue by the ZnO/g-C_3N_4 composite.[16]

Stability Test. The stability of the ZnO/g-C_3N_4 composite is an important factor for its practical application into the bisphenol degradation. The stability of the ZnO/g-C_3N_4 composite system was investigated through the reusability test for 3 cycles toward degradation of BPE. It was clearly found that after three cycles of reusability, the degradation ability of the composite slightly decreased (Figure S11). The results were attributed to the chemical and photostability of the composite.[44] From SEM, TEM, PL, DRS, XRD, and FTIR analysis, it was also found that the properties of the composite did not change after the photocatalytic reaction. The results confirmed the chemical stability of the composite.

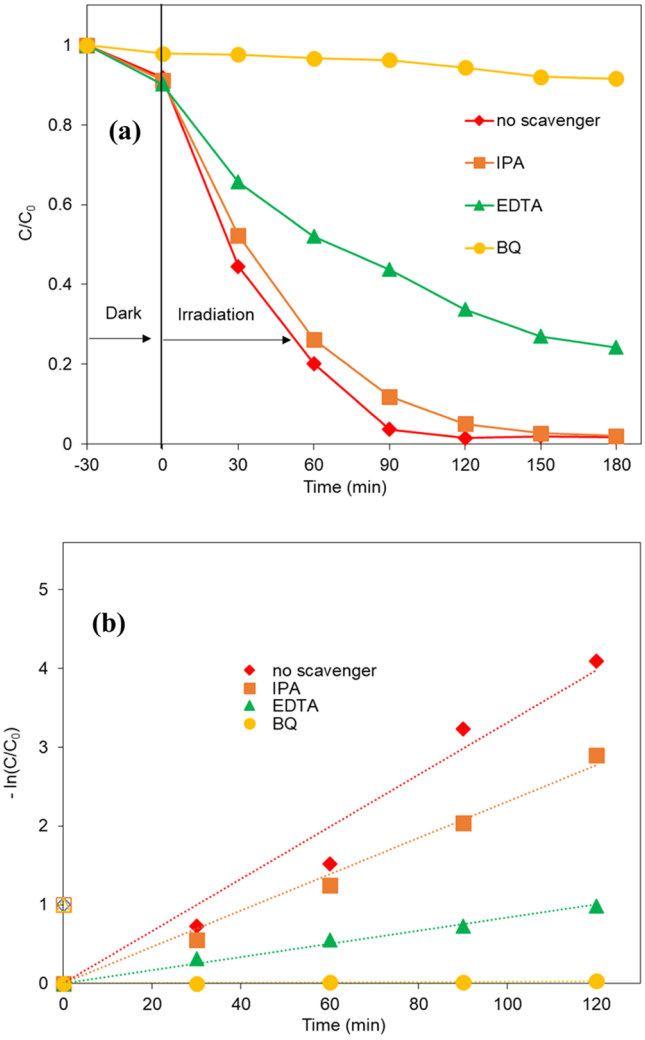

Figure 7. (a) Effect of scavenger role on the photocatalytic degradation of BPE with the ZnO/g-C_3N_4 composite and (b) plot of $-\ln(C/C_0)$ versus irradiation time; BPE: 3 ppm (30 mL), photocatalyst: 30 mg.

Table 3. Effect of Scavenger Role on the Kinetic Parameters for Photocatalytic Degradation of BPE with the ZnO/g-C_3N_4 Composite

scavenger	rate constant (min^{-1})	$T_{1/2}$ (min)	R^2
without	3.3×10^{-2}	21	0.97
IPA	2.3×10^{-2}	30	0.99
EDTA	8.4×10^{-3}	83	0.99
BQ	3.0×10^{-4}	2310	0.87

Mechanism. In the ZnO/g-C_3N_4 composite, the electrons in the g-C_3N_4 were spontaneously transferred to the ZnO through the interface until their Fermi level energies reached equilibrium.[58,59] It is assumed that an intermediate band in the

https://doi.org/10.1021/acsomega.2c06678
ACS Omega 2023, 8, 11824−11836

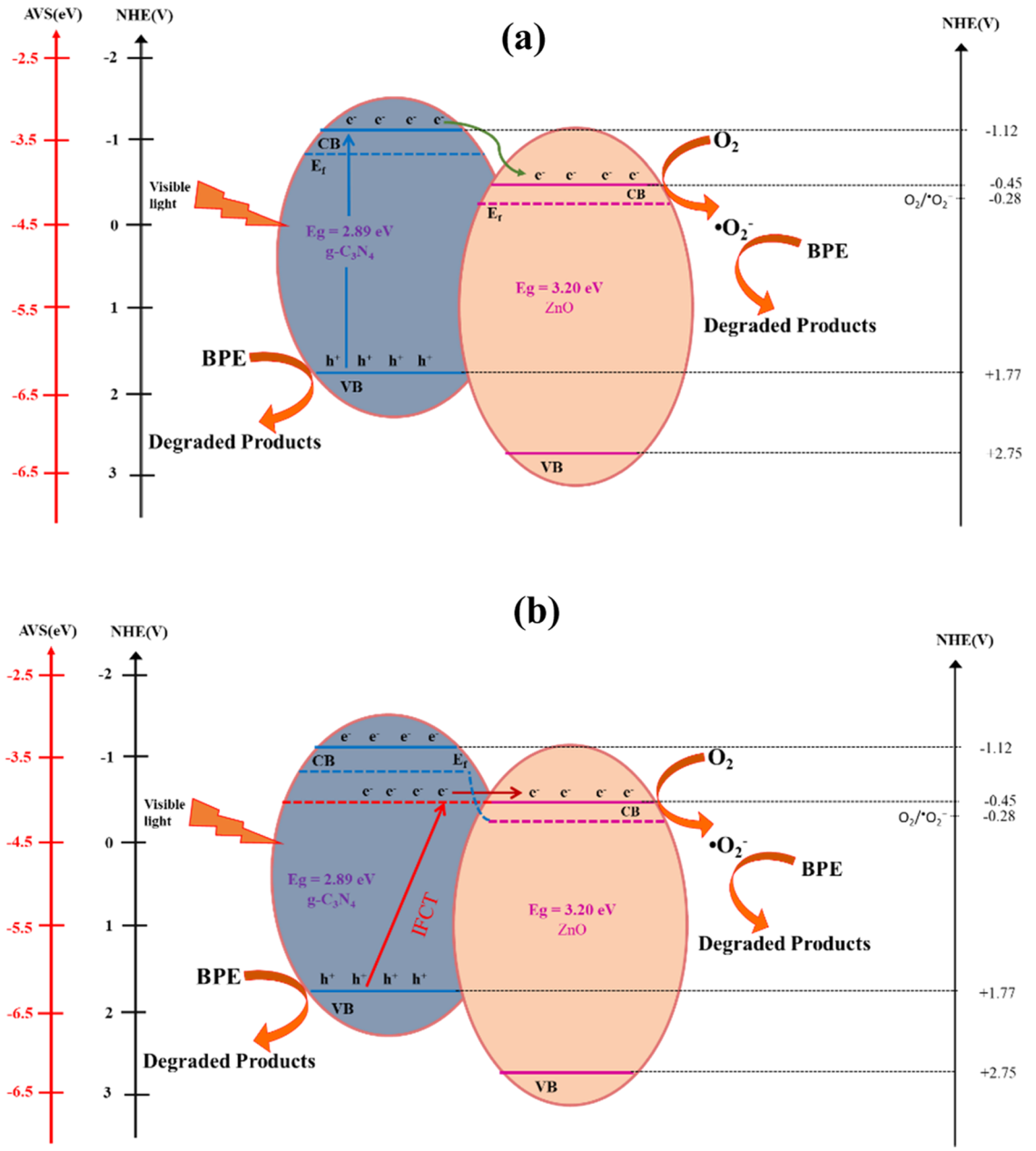

Figure 8. (a) Conventional charge transfer mechanism and (b) IFCT mechanism for photocatalytic degradation of BPE with the ZnO/g-C_3N_4 composite.

mid band gap exists in the composite due to Fermi level energy equilibrium and that the position of the intermediate energy band is equal to the conductance band edge potential (E_{CB}) of ZnO. Furthermore, the VBXPS analysis indicated that the VB position of the composite was 1.88 eV (Figure S12). The valence band edge potential (E_{VB}) of the composite was estimated according to the eq 4.[60]

$$E_{NHE}/V = \Phi_{WF} + \Phi_{sample} - 4.44 \quad (4)$$

where E_{NHE}, Φ_{WF}, and Φ_{sample} are the VB potential of the photocatalyst, electron work function of the analyzer (4.33 eV), and VB position of the photocatalyst (eV) determined using VBXPS, respectively. The E_{VB} of the composite was estimated at 1.77 eV. The E_{CB} of g-C_3N_4 and the intermediate energy band position of the composite were estimated according to eq 5 and the DRS result of the band gap of g-C_3N_4 and the composite.[60]

$$E_{CB} = E_{VB} - E_g \quad (5)$$

where E_g is the band gap of the semiconductor. The E_{CB} of g-C_3N_4 and the intermediate band energy position of the composite were determined as −1.12 and −0.45 eV, respectively. Since the intermediate energy band position and E_{CB} of ZnO were equal, the E_{CB} and E_{VB} of ZnO were estimated at −0.45 and 2.75 eV, respectively.

Two possible mechanisms can be proposed for the photocatalytic degradation of BPE with the ZnO/g-C_3N_4 composite. Firstly, the conventional charge transfer mechanism is proposed, as shown in Figure 8a. Electrons in g-C_3N_4 are excited to the CB, while the holes are created in the VB upon the visible light irradiation. The value of the E_{CB} of g-C_3N_4 is

https://doi.org/10.1021/acsomega.2c06678
ACS Omega 2023, 8, 11824−11836

more negative than that of ZnO. Hence, the photogenerated electrons are shifted to the CB of ZnO, which are further promoted to the surface. Thus, the recombination of e^-/h^+ pairs can be reduced. Secondly, the interfacial charge transfer mechanism (IFCT) is proposed, as shown in Figure 8b. Photogenerated electrons are transferred from the VB of g-C_3N_4 to the intermediate energy band of the composite through the IFCT mechanism. Then, the electrons are shifted to the CB of ZnO. Thus, the photogenerated charge separation may improve.

Due to the CB position of ZnO being more negative than the standard reduction potential of $O_2/{}^{\bullet}O_2^-$ (−0.28 eV), O_2 in the environment reacts with the photogenerated electrons to produce ${}^{\bullet}O_2^-$ radicals. Therefore, ${}^{\bullet}O_2^-$ radicals are the major and efficient active species for degradation of BPE. In contrast, the generated holes in g-C_3N_4 are not able to react with H_2O to produce ${}^{\bullet}OH$ radicals due to the VB position of g-C_3N_4 being less positive compared to the standard redox potential of $H_2O/{}^{\bullet}OH$ (2.27 eV).[22] Therefore, BPE is directly oxidized by the holes. The relevant photocatalytic reactions of degradation of BPE with the ZnO/g-C_3N_4 composite under visible light irradiation are expressed as follows:

$$\text{g-}C_3N_4 + \text{visible light} \rightarrow \text{g-}C_3N_4(e^-) + \text{g-}C_3N_4(h^+) \quad (6)$$

$$\text{g-}C_3N_4(e^-) + \text{ZnO} \rightarrow \text{ZnO}(e^-) + \text{g-}C_3N_4 \quad (7)$$

$$O_2 + \text{ZnO}(e^-) \rightarrow \text{ZnO} + {}^{\bullet}O_2^- \quad (8)$$

$$\text{BPE} + {}^{\bullet}O_2^- \rightarrow \text{degraded products} \quad (9)$$

$$\text{BPE} + h^+ \rightarrow \text{degraded products} \quad (10)$$

CONCLUSIONS

Cheap and nontoxic ZnO, g-C_3N_4, and the ZnO/g-C_3N_4 composite were synthesized by the facile calcination method. The formation of the composite was confirmed by FTIR, XPS, SEM, and TEM analysis. The higher absorption ability of the visible light of the composite was detected by UV−vis DRS analysis. The decrement of the photogenerated electron−hole pair recombination was evaluated by PL and EIS investigation. As a result, the composite showed admirable photocatalytic activity on degradation of BPE. Two possible mechanisms for the photocatalytic reaction have been proposed.

ASSOCIATED CONTENT

Supporting Information

The Supporting Information is available free of charge at https://pubs.acs.org/doi/10.1021/acsomega.2c06678.

XRD patterns, elemental mapping, nitrogen adsorption−desorption isotherm and pore size distribution curve, and tauc plots of photocatalysts; photocatalytic degradation of BPE with photocatalysts at different conditions, and Schematic synthetic diagram of ZnO/g-C_3N_4 composite and reusability of ZnO/g-C_3N_4 composite (PDF)

AUTHOR INFORMATION

Corresponding Authors

Mahmudul Hassan Suhag − *Department of Chemistry for Materials, Graduate School of Engineering, Mie University, Tsu, Mie 514-8507, Japan; Department of Chemistry, University of Barishal, Barishal 8254, Bangladesh;* orcid.org/0000-0001-9214-3946; Email: suhag.che057@gmail.com

Satoshi Kaneco − *Department of Chemistry for Materials, Graduate School of Engineering, Mie University, Tsu, Mie 514-8507, Japan;* orcid.org/0000-0002-6653-2312; Email: kaneco@chem.mie-u.ac.jp

Authors

Aklima Khatun − *Department of Chemistry for Materials, Graduate School of Engineering, Mie University, Tsu, Mie 514-8507, Japan*

Ikki Tateishi − *Environmental Preservation Center, Mie University, Tsu, Mie 514-8507, Japan*

Mai Furukawa − *Department of Chemistry for Materials, Graduate School of Engineering, Mie University, Tsu, Mie 514-8507, Japan*

Hideyuki Katsumata − *Department of Chemistry for Materials, Graduate School of Engineering, Mie University, Tsu, Mie 514-8507, Japan;* orcid.org/0000-0002-4634-4998

Complete contact information is available at: https://pubs.acs.org/10.1021/acsomega.2c06678

Author Contributions

M.H.S.: conceptualization, methodology, data curation, formal analysis, investigation, writing—original draft, and writing—review and editing. A.K.: formal analysis, and writing—review and editing. I.T.: formal analysis, and writing—review and editing. M.F.: formal analysis, and writing—review and editing. H.K.: writing—review and editing. S.K.: writing—review, editing, and supervision.

Notes

The authors declare no competing financial interest.

ACKNOWLEDGMENTS

This research work was partially funded by the Grant-in-Aid for Scientific Research (B) 21H03642 from the Ministry of Education, Culture, Sports, Science, and Technology of Japan.

REFERENCES

(1) Tian, B.; Wu, N.; Pan, X.; Wang, Z.; Yan, C.; Sharma, V. K.; Qu, R. Ferrate(VI) Oxidation of Bisphenol E−Kinetics, Removal Performance, and Dihydroxylation Mechanism. *Water Res.* **2022**, *210*, No. 118025.

(2) Savage, P. E.; Hunter, S. E.; Hoffee, K. L.; Schuelke, T. J.; Smith, M. J. Bisphenol E Decomposition in High-Temperature Water. *Ind. Eng. Chem. Res.* **2006**, *45*, 7775−7780.

(3) Garg, R.; Gupta, R.; Bansal, A. Synthesis of g-C_3N_4/ZnO Nanocomposite for Photocatalytic Degradation of a Refractory Organic Endocrine Disrupter. *Mater. Today Proc.* **2021**, *44*, 855−859.

(4) Uzzaman, M.; Hasan, M. K.; Mahmud, S.; Yousuf, A.; Islam, S.; Uddin, M. N.; Barua, A. Physicochemical, Spectral, Molecular Docking and ADMET Studies of Bisphenol Analogues; A Computational Approach. *Inf. Med. Unlocked* **2021**, *25*, No. 100706.

(5) Reddy, P. V. L.; Kim, K.-H.; Kavitha, B.; Kumar, V.; Raza, N.; Kalagara, S. Photocatalytic Degradation of Bisphenol A in Aqueous Media: A Review. *J. Environ. Manage.* **2018**, *213*, 189−205.

(6) Pozdnyakov, I. P.; Guo, L.; Glebov, E. M.; Wu, F.; Plyusnin, V. F.; Grivin, V. P.; Deng, N. Aqueous Photochemistry of Bisphenol E in the Presence of β-Cyclodextrin. *High Energy Chem.* **2011**, *45*, 214−221.

(7) Amaterz, E.; Bouddouch, A.; Tara, A.; Taoufyq, A.; Bakiz, B.; Benlhachemi, A.; Jbara, O. Electrochemical Degradation of Bisphenol A Using Electrodeposited $SrHPO_4$ Thin Films. *Nanotechnol. Environ. Eng.* **2021**, *6*, 18.

(8) Lei, Y.-Q.; He, Z.-X.; Luo, Y.; Lu, S.-N.; Li, C.-J. Chemical Degradation of Bisphenol A Diglycidyl Ether/Methyl Tetrahydrophthalic Anhydride Networks by p-Toluenesulfonic-Acetic Anhydride. *Polym. Degrad. Stab.* **2016**, *123*, 115−120.
(9) Zhou, N.; Liu, Y.; Cao, S.; Guo, R.; Ma, Y.; Chen, J. Biodegradation of Bisphenol Compounds in the Surface Water of Taihu Lake and the Effect of Humic Acids. *Sci. Total Environ.* **2020**, *723*, No. 138146.
(10) Kaneco, S.; Rahman, M. A.; Suzuki, T.; Katsumata, H.; Ohta, K. Optimization of Solar Photocatalytic Degradation Conditions of Bisphenol A in Water Using Titanium Dioxide. *J. Photochem. Photobiol., A* **2004**, *163*, 419−424.
(11) Wang, Y.; Hu, K.; Yang, Z.; Ye, C.; Li, X.; Yan, K. Facile Synthesis of Porous ZnO Nanoparticles Efficient for Photocatalytic Degradation of Biomass-Derived Bisphenol A Under Simulated Sunlight Irradiation. *Front. Bioeng. Biotechnol.* **2021**, *8*, No. 616780.
(12) Paul, D. R.; Gautam, S.; Panchal, P.; Nehra, S. P.; Choudhary, P.; Sharma, A. ZnO-Modified g-C_3N_4: A Potential Photocatalyst for Environmental Application. *ACS Omega* **2020**, *5*, 3828−3838.
(13) Ngullie, R. C.; Alaswad, S. O.; Bhuvaneswari, K.; Shanmugam, P.; Pazhanivel, T.; Arunachalam, P. Synthesis and Characterization of Efficient ZnO/g-C_3N_4 Nanocomposites Photocatalyst for Photocatalytic Degradation of Methylene Blue. *Coatings* **2020**, *10*, 500.
(14) Ismael, M. The Photocatalytic Performance of the ZnO/g-C_3N_4 Composite Photocatalyst toward Degradation of Organic Pollutants and Its Inactivity toward Hydrogen Evolution: The Influence of Light Irradiation and Charge Transfer. *Chem. Phys. Lett.* **2020**, *739*, No. 136992.
(15) Pérez-Molina, Á.; Pastrana-Martínez, L. M.; Pérez-Poyatos, L. T.; Morales-Torres, S.; Maldonado-Hódar, F. J. One-Pot Thermal Synthesis of g-C_3N_4/ZnO Composites for the Degradation of 5-Fluoruracil Cytostatic Drug under UV-LED Irradiation. *Nanomaterials* **2022**, *12*, 340.
(16) Zhang, S.; Su, C.; Ren, H.; Li, M.; Zhu, L.; Ge, S.; Wang, M.; Zhang, Z.; Li, L.; Cao, X. In-Situ Fabrication of g-C_3N_4/ZnO Nanocomposites for Photocatalytic Degradation of Methylene Blue: Synthesis Procedure Does Matter. *Nanomaterials* **2019**, *9*, 215.
(17) Zhou, J.; Zhang, M.; Zhu, Y. Preparation of Visible Light-Driven g-C_3N_4@ZnO Hybrid Photocatalyst via Mechanochemistry. *Phys. Chem. Chem. Phys.* **2014**, *16*, 17627−17633.
(18) Ravichandran, K.; Kalpana, K.; Ibrahim, M. M.; Seelan, K. S. Effect of Source Material of g-C_3N_4 on the Photocatalytic Activity of ZnO/g-C_3N_4 thin Film Coated on Stainless Steel Mesh Substrate. *Mater. Today: Proc.* **2019**, *48*, 207−215.
(19) Li, L.; Sun, S.-Q.; Wang, Y.-X.; Wang, C.-Y. Facile Synthesis of ZnO/g-C_3N_4 Composites with Honeycomb-like Structure by H_2 Bubble Templates and Their Enhanced Visible Light Photocatalytic Performance. *J. Photochem. Photobiol., A* **2018**, *355*, 16−24.
(20) Sun, Q.; Sun, Y.; Zhou, M.; Cheng, H.; Chen, H.; Dorus, B.; Lu, M.; Le, T. A 2D/3D g-C_3N_4/ZnO Heterojunction Enhanced Visible-Light Driven Photocatalytic Activity for Sulfonamides Degradation. *Ceram. Int.* **2022**, *48*, 7283−7290.
(21) Uma, R.; Ravichandran, K.; Sriram, S.; Sakthivel, B. Cost-Effective Fabrication of ZnO/g-C_3N_4 Composite Thin Films for Enhanced Photocatalytic Activity against Three Different Dyes (MB, MG and RhB). *Mater. Chem. Phys.* **2017**, *201*, 147−155.
(22) Zhang, Z.; Sun, Y.; Wang, Y.; Yang, Y.; Wang, P.; Shi, L.; Feng, L.; Fang, S.; Liu, Q.; Ma, L.; Peng, S.; Wang, T. Synthesis and Photocatalytic Activity of g-C_3N_4/ZnO Composite Microspheres under Visible Light Exposure. *Ceram. Int.* **2022**, *48*, 3293−3302.
(23) Zhong, Q.; Lan, H.; Zhang, M.; Zhu, H.; Bu, M. Preparation of Heterostructure g-C_3N_4/ZnO Nanorods for High Photocatalytic Activity on Different Pollutants (MB, RhB, Cr(VI) and Eosin). *Ceram. Int.* **2020**, *46*, 12192−12199.
(24) Kumaresan, N.; Sinthiya, M. M. A.; Sarathbavan, M.; Ramamurthi, K.; Sethuraman, K.; Babu, R. R. Synergetic Effect of g-C_3N_4/ZnO Binary Nanocomposites Heterojunction on Improving Charge Carrier Separation through 2D/1D Nanostructures for Effective Photocatalytic Activity under the Sunlight Irradiation. *Sep. Purif. Technol.* **2020**, *244*, No. 116356.
(25) Zhang, Y.; Liu, H.; Gao, F.; Tan, X.; Cai, Y.; Hu, B.; Huang, Q.; Fang, M.; Wang, X. Application of MOFs and COFs for Photocatalysis in CO_2 Reduction, H_2 Generation, and Environmental Treatment. *EnergyChem* **2022**, *4*, No. 100078.
(26) Liu, X.; Verma, G.; Chen, Z.; Hu, B.; Huang, Q.; Yang, H.; Ma, S.; Wang, X. Metal-Organic Framework Nanocrystal-Derived Hollow Porous Materials: Synthetic Strategies and Emerging Applications. *Innovation* **2022**, *3*, No. 100281.
(27) Kumar Kuila, S.; Kumbhakar, P.; Sekhar Tiwary, C.; Kumar Kundu, T. Photon and Vibration Synergism on Planar Defects Induced 2D-Graphitic Carbon Nitride for Ultrafast Remediation of Dyes and Antibiotic Ampicillin. *J. Mater. Sci.* **2022**, *57*, 8658−8675.
(28) Kuila, S. K.; Sarkar, R.; Kumbhakar, P.; Kumbhakar, P.; Tiwary, C. S.; Kundu, T. K. Photocatalytic Dye Degradation under Sunlight Irradiation Using Cerium Ion Adsorbed Two-Dimensional Graphitic Carbon Nitride. *J. Environ. Chem. Eng.* **2020**, *8*, No. 103942.
(29) de Sousa, J. G. M.; da Silva, T. V. C.; de Moraes, N. P.; da Silva, M. L. C. P.; Rocha, R.; da, S.; Landers, R.; Rodrigues, L. A. Visible Light-Driven ZnO/g-C_3N_4 /Carbon Xerogel Ternary Photocatalyst with Enhanced Activity for 4-Chlorophenol Degradation. *Mater. Chem. Phys.* **2020**, *256*, No. 123651.
(30) Zhang, S.; Liu, Y.; Ma, R.; Jia, D.; Wen, T.; Ai, Y.; Zhao, G.; Fang, F.; Hu, B.; Wang, X. Molybdenum (VI)-Oxo Clusters Incorporation Activates g-C_3N_4 with Simultaneously Regulating Charge Transfer and Reaction Centers for Boosting Photocatalytic Performance. *Adv. Funct. Mater.* **2022**, *32*, No. 2204175.
(31) Liu, W.; Wang, M.; Xu, C.; Chen, S. Facile Synthesis of g-C_3N_4/ZnO Composite with Enhanced Visible Light Photooxidation and Photoreduction Properties. *Chem. Eng. J.* **2012**, *209*, 386−393.
(32) Guan, R.; Li, J.; Zhang, J.; Zhao, Z.; Wang, D.; Zhai, H.; Sun, D. Photocatalytic Performance and Mechanistic Research of ZnO/g-C_3N_4 on Degradation of Methyl Orange. *ACS Omega* **2019**, *4*, 20742−20747.
(33) Kumbhakar, P.; Pramanik, A.; Biswas, S.; Kole, A. K.; Sarkar, R.; Kumbhakar, P. In-Situ Synthesis of RGO-ZnO Nanocomposite for Demonstration of Sunlight Driven Enhanced Photocatalytic and Self-Cleaning of Organic Dyes and Tea Stains of Cotton Fabrics. *J. Hazard. Mater.* **2018**, *360*, 193−203.
(34) Prasad Adhikari, S.; Pant, H. R.; Kim, H. J.; Park, C. H.; Kim, C. S. Deposition of ZnO Flowers on the Surface of g-C_3N_4 Sheets via Hydrothermal Process. *Ceram. Int.* **2015**, *41*, 12923−12929.
(35) Kumar, K. V. A.; Vinodkumar, T.; Selvaraj, M.; Suryakala, D.; Subrahmanyam, C. Visible Light-Induced Catalytic Abatement of 4-Nitrophenol and Rhodamine B Using ZnO/g-C_3N_4 Catalyst. *J. Chem. Sci.* **2021**, *133*, 41.
(36) Wang, Y.; Shi, R.; Lin, J.; Zhu, Y. Enhancement of Photocurrent and Photocatalytic Activity of ZnO Hybridized with Graphite-like C_3N_4. *Energy Environ. Sci.* **2011**, *4*, 2922−2929.
(37) Liu, W.; Wang, M.; Xu, C.; Chen, S.; Fu, X. Significantly Enhanced Visible-Light Photocatalytic Activity of g-C_3N_4 via ZnO Modification and the Mechanism Study. *J. Mol. Catal. A: Chem.* **2013**, *368*−*369*, 9−15.
(38) Qin, J.; Yang, C.; Cao, M.; Zhang, X.; Saravanan, R.; Limpanart, S.; Ma, M.; Liu, R. Two-Dimensional Porous Sheet-like Carbon-Doped ZnO/g-C_3N_4 nanocomposite with High Visible-Light Photocatalytic Performance. *Mater. Lett.* **2017**, *189*, 156−159.
(39) Wang, J.; Yang, Z.; Gao, X.; Yao, W.; Wei, W.; Chen, X.; Zong, R.; Zhu, Y. Core-Shell g-C_3N_4@ZnO Composites as Photoanodes with Double Synergistic Effects for Enhanced Visible-Light Photoelectrocatalytic Activities. *Appl. Catal., B* **2017**, *217*, 169−180.
(40) Naseri, A.; Samadi, M.; Pourjavadi, A.; Ramakrishna, S.; Moshfegh, A. Z. Enhanced Photocatalytic Activity of ZnO/g-C_3N_4 Nanofibers Constituting Carbonaceous Species under Simulated Sunlight for Organic Dye Removal. *Ceram. Int.* **2021**, *47*, 26185−26196.
(41) Park, T. J.; Pawar, R. C.; Kang, S.; Lee, C. S. Ultra-Thin Coating of g-C_3N_4 on an Aligned ZnO Nanorod Film for Rapid

https://doi.org/10.1021/acsomega.2c06678
ACS Omega 2023, 8, 11824−11836

Charge Separation and Improved Photodegradation Performance. *RSC Adv.* **2016**, *6*, 89944−89952.
(42) Li, X.; Li, M.; Yang, J.; Li, X.; Hu, T.; Wang, J.; Sui, Y.; Wu, X.; Kong, L. Synergistic Effect of Efficient Adsorption g-C_3N_4/ZnO Composite for Photocatalytic Property. *J. Phys. Chem. Solids* **2014**, *75*, 441−446.
(43) Fu, J.; Yu, J.; Jiang, C.; Cheng, B. g-C_3N_4-Based Heterostructured Photocatalysts. *Adv. Energy Mater.* **2018**, *8*, No. 1701503.
(44) Gayathri, M.; Sakar, M.; Satheeshkumar, E.; Sundaravadivel, E. Insights into the Mechanism of ZnO/g-C_3N_4 Nanocomposites toward Photocatalytic Degradation of Multiple Organic Dyes. *J. Mater. Sci. Mater. Electron.* **2022**, *33*, 9347−9357.
(45) Zong, H.; Zhao, T.; Zhou, G.; Qian, R.; Feng, T.; Pan, J. H. Revisiting Structural and Photocatalytic Properties of g-C_3N_4/TiO_2: Is Surface Modification of TiO_2 by Calcination with Urea an Effective Route to "Solar" Photocatalyst? *Catal. Today* **2019**, *335*, 252−261.
(46) Dong, J.; Zhang, Y.; Hussain, M. I.; Zhou, W.; Chen, Y.; Wang, L. N. g-C_3N_4: Properties, Pore Modifications, and Photocatalytic Applications. *Nanomaterials* **2022**, *12*, 121.
(47) Lee, S.; Jeong, S.; Kim, D.; Hwang, S.; Jeon, M.; Moon, J. ZnO Nanoparticles with Controlled Shapes and Sizes Prepared Using a Simple Polyol Synthesis. *Superlattices Microstruct.* **2008**, *43*, 330−339.
(48) Molla, M. A. I.; Furukawa, M.; Tateishi, I.; Katsumata, H.; Suzuki, T.; Kaneco, S. Photocatalytic Decolorization of Dye with Self-Dye-Sensitization under Fluorescent Light Irradiation. *ChemEngineering* **2017**, *1*, 8.
(49) Moussa, H.; Chouchene, B.; Gries, T.; Balan, L.; Mozet, K.; Medjahdi, G.; Schneider, R. Growth of ZnO Nanorods on Graphitic Carbon Nitride GCN Sheets for the Preparation of Photocatalysts with High Visible-Light Activity. *ChemCatChem* **2018**, *10*, 4973−4983.
(50) Zhu, Y.-P.; Li, M.; Liu, Y.-L.; Ren, T.-Z.; Yuan, Z.-Y. Carbon-Doped ZnO Hybridized Homogeneously with Graphitic Carbon Nitride Nanocomposites for Photocatalysis. *J. Phys. Chem. C* **2014**, *118*, 10963−10971.
(51) Jingyu, H.; Ran, Y.; Zhaohui, L.; Yuanqiang, S.; Lingbo, Q.; Kani, A. N. In-Situ Growth of ZnO Globular on g-C_3N_4 to Fabrication Binary Heterojunctions and Their Photocatalytic Degradation Activity on Tetracyclines. *Solid State Sci.* **2019**, *92*, 60−67.
(52) Liu, J.; Zhang, T.; Wang, Z.; Dawson, G.; Chen, W. Simple Pyrolysis of Urea into Graphitic Carbon Nitride with Recyclable Adsorption and Photocatalytic Activity. *J. Mater. Chem.* **2011**, *21*, 14398−14401.
(53) Yue, B.; Li, Q.; Iwai, H.; Kako, T.; Ye, J. Hydrogen Production Using Zinc-Doped Carbon Nitride Catalyst Irradiated with Visible Light. *Sci. Technol. Adv. Mater.* **2011**, *12*, No. 034401.
(54) Islam, J. B.; Islam, M. R.; Furukawa, M.; Tateishi, I.; Katsumata, H.; Kaneco, S. Ag-Modified g-C_3N_4 with Enhanced Activity for the Photocatalytic Reduction of Hexavalent Chromium in the Presence of EDTA under Ultraviolet Irradiation. *Environ. Technol.* **2022**, DOI: 10.1080/09593330.2022.2068379.
(55) Xing, H.; Ma, H.; Fu, Y.; Xue, M.; Zhang, X.; Dong, X.; Zhang, X. Preparation of g-C_3N_4/ZnO Composites and Their Enhanced Photocatalytic Activity. *Mater. Technol.* **2015**, *30*, 122−127.
(56) Yang, P.; Wang, J.; Yue, G.; Yang, R.; Zhao, P.; Yang, L.; Zhao, X.; Astruc, D. Constructing Mesoporous g-C_3N_4/ZnO Nanosheets Catalyst for Enhanced Visible-Light Driven Photocatalytic Activity. *J. Photochem. Photobiol., A* **2020**, *388*, No. 112169.
(57) Yu, W.; Xu, D.; Peng, T. Enhanced Photocatalytic Activity of g-C_3N_4 for Selective CO_2 Reduction to CH_3OH via Facile Coupling of ZnO: A Direct Z-Scheme Mechanism. *J. Mater. Chem. A* **2015**, *3*, 19936−19947.
(58) Liao, G.; Li, C.; Li, X.; Fang, B. Emerging Polymeric Carbon Nitride Z-Scheme Systems for Photocatalysis. *Cell Rep. Phys. Sci.* **2021**, No. 100355.
(59) Lu, X.; Quan, L.; Hou, H.; Qian, J.; Liu, Z.; Zhang, Q. Fabrication of 1D/2D Y-Doped CeO_2/$ZnIn_2S_4$ S-Scheme Photocatalyst for Enhanced Photocatalytic H_2 Evolution. *J. Alloys Compd.* **2022**, *925*, No. 166552.
(60) Katsumata, H.; Islam Molla, M. A.; Islam, J. B.; Tateishi, I.; Furukawa, M.; Kaneco, S. Dual Z-Scheme Heterojunction g-C_3N_4/Ag_3PO_4/AgBr Photocatalyst with Enhanced Visible-Light Photocatalytic Activity. *Ceram. Int.* **2022**, *48*, 21939−21946.

https://doi.org/10.1021/acsomega.2c06678
ACS Omega 2023, 8, 11824−11836